

Electronic Supplementary Information

Tuning the properties of *tris*(hydroxypyridinone) ligands: efficient ^{68}Ga chelators for PET imaging

Content

S.1 THP^{Me} radiolabelling

S.2 THP^{Me} *in vivo* radiolabelling experiment

Table S1-S2 Measured complex formation constants for THP^{Me} and THP^H

Figure S1 Chemical structures of selected Ga³⁺ chelators evaluated for use with ^{68}Ga .

Figure S2, S3 HPLC characterisation of THP^H and THPO (additional UV chromatograms)

Figure S4 [^{nat}Ga(THP^H)] mass spectrum

Figure S5 Absorbance spectra of THP ligands

Figure S6 ¹H NMR spectrum of an equimolar mixture of THP^H and THP^{Me}

Figure S7 Serum stability of [⁶⁷Ga(THP^H)]

Figure S8 *In vivo* behaviour of THP^{Me}

Figure S9-S16 ¹H NMR and ¹³C NMR of compounds 2-9

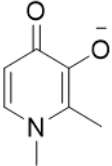
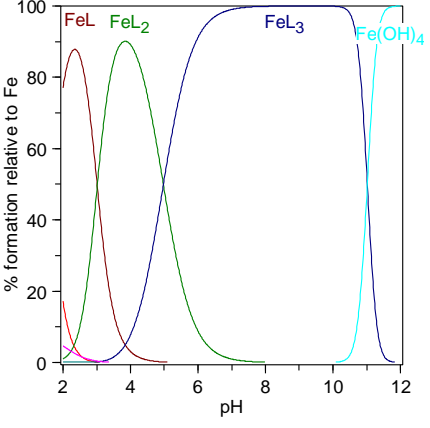
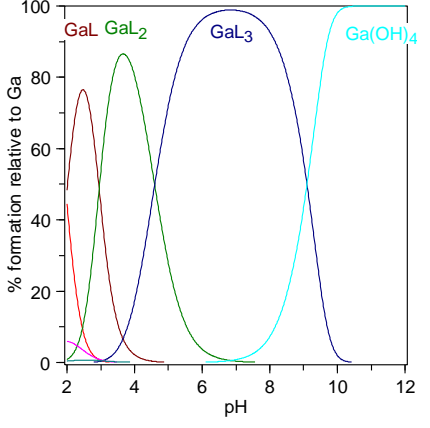
S.1 THP^{Me} radiolabelling

An E&Z generator was eluted with 5 mL of pure HCl 0.1 M (Fluka analytical) in five 1 mL fractions and their activity measured by a Capintec radionuclide dose calibrator. An aliquot of the highest activity fraction (100 μ L, 15-20 MBq) was mixed with THP^{Me} (100 μ L, concentration range 200-2 μ M) in ammonium acetate 0.5 M. Verification of the radiolabelling was carried out after 5 minutes by reversed-phase HPLC (method 7: Mobile phase A: H₂O + 0.1% TFA, B: MeCN + 0.1% TFA, % B increased from 2% at 5 minutes to 90% at 25 minutes and back to 2% at 27 minutes) and iTLC-SG (mobile phase 1: R_f [Ga(THP^{Me})] = 0, R_f Ga_{colloid} = 0, R_f ⁶⁸Ga_{free} = 1; mobile phase 2: R_f [Ga(THP^{Me})] = 1, R_f ⁶⁸Ga_{free} = 0, ⁶⁸Ga_{colloid} = 0). Quantitative radiolabelling was obtained for all examined concentrations. A single peak was obtained in the radiochromatogram at 15 min 28 s (**Figure S8B**, upper panel). Radiolabelling of THP^{Me} at 0.1 μ M was performed using a second E&Z generator, eluted with clinical grade 0.1 M HCl (E&Z).

S.2 THP^{Me} *in vivo* radiolabelling experiment

A female BALB/c mouse (22 g, 9 weeks, Charles Rivers) was anaesthetised with isoflurane (O₂ flow rate of 1.0-1.5 L/min and isoflurane levels of 2-2.5%), cannulated using a catheter (25 μ L volume) and subjected to a CT scan. Subsequently, a PET scan was started, and the mouse injected with acetate buffered ⁶⁸Ga (150 μ L, 0.1 M ammonium acetate, 8.12 MBq) while scanning, followed at 45 minutes by an injection of THP^{Me} (100 μ L of a 24 μ M solution in PBS). Upon completion of the scans, the animal was sacrificed by neck dislocation whilst anaesthetised and the urine was collected and analysed by reversed-phase HPLC (method 7). Similar to what was observed for THP^H, THP^{Me} was able to bind ⁶⁸Ga *in vivo* thus accelerating its blood clearance (**Figure S8A**), and HPLC analysis of mouse urine (**Figure S8B**) revealed quantitative formation of the [⁶⁸Ga(THP^{Me})] complex. These data confirm previous *in vitro* studies demonstrating the ability of THP^{Me} to transchelate transferrin-bound Ga(III).¹

Table S1. Formation constants for the Ga(III) and Fe(III) complexes of deferiprone. Detailed species and chemical equations for which the complex formation constants were determined are defined below. Speciation plots for $[L]_{total} = 10 \mu\text{M}$ and $[M]_{total} = 1 \mu\text{M}$ are also reported.

Deferiprone	
$L = $ 	
Chemical equilibrium equations	
$M^{3+} + L^{-} \rightleftharpoons [ML]^{2+}$	$Log \beta_{[ML]^{2+}}$
$M^{3+} + 2 L^{-} \rightleftharpoons [ML_2]^{+}$	$Log \beta_{[ML_2]^{+}}$
$M^{3+} + 3 L^{-} \rightleftharpoons [ML_3]$	$Log \beta_{[ML_3]}$
$M^{3+} + 4 OH^{-} \rightleftharpoons [M(OH)_4]^{-}$	$Log \beta_{[M(OH)_4]^{-}}$
Complex formation constants	
$Log \beta_{[FeL]^{2+}}$	15.0 *
$Log \beta_{[FeL_2]^{+}}$	27.5 *
$Log \beta_{[FeL_3]}$	37.5 *
$Log \beta_{[Fe(OH)_4]^{-}}$	34.4 ²
pFe	20.8
$Log \beta_{[GaL]^{2+}}$	14.4 *
$Log \beta_{[GaL_2]^{+}}$	27.0*
$Log \beta_{[GaL_3]}$	37.4 *
$Log \beta_{[Ga(OH)_4]^{-}}$	39.4 ²
pGa	20.7
Speciation plots	
	

* Stability constants for deferiprone have been previously reported in the literature;³ measurements have been repeated here as a control to verify the accuracy of our titration methods.

Table S2. Conditional formation constants for the Ga(III) and Fe(III) complexes of THP^{Me}. Detailed species and chemical equations for which the constants were determined are defined below. Speciation plots for $[L]_{total} = 10 \mu M$ and $[M]_{total} = 1 \mu M$ are also reported.

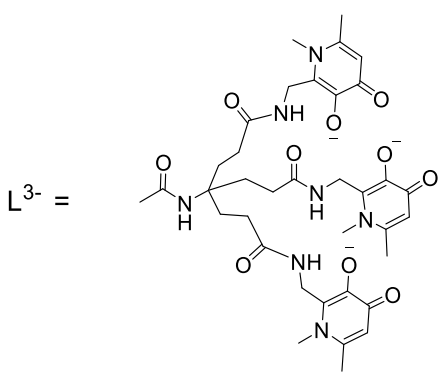
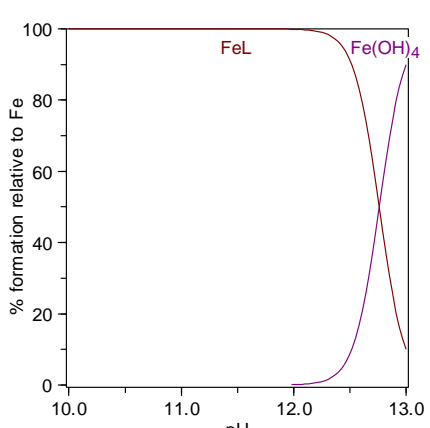
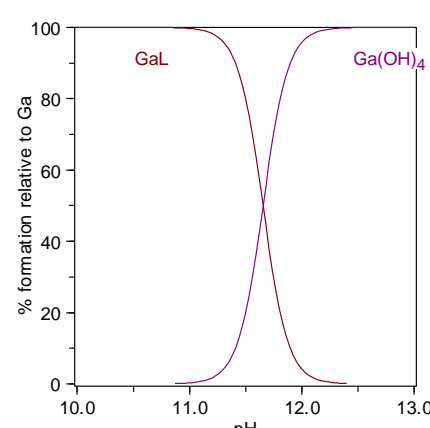
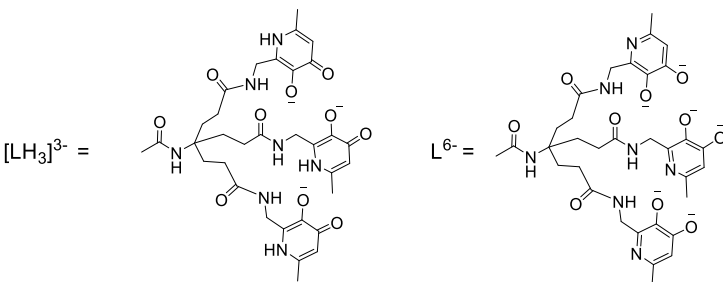
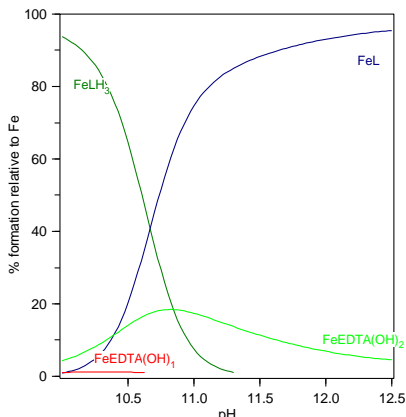
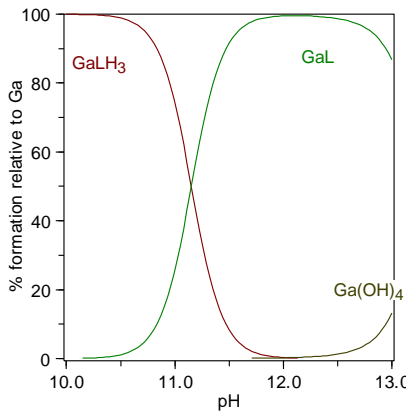
THP^{Me}	
 <p>$L^{3-} =$</p>	
Chemical equilibrium equations	
$M^{3+} + L^{3-} \rightleftharpoons [ML]$ $M^{3+} + 4 OH^- \rightleftharpoons [M(OH)_4]^-$	$\text{Log } \beta_{[ML]}$ $\text{Log } \beta_{[M(OH)_4]}^-$
Conditional formation constants	
$\text{Log } \beta_{[FeL]} \quad 34.2$ $\text{Log } \beta_{[Fe(OH)_4]}^- \quad 34.4^2$ $\text{pFe} \quad 29.1$	$\text{Log } \beta_{[GaL]} \quad 35.0$ $\text{Log } \beta_{[Ga(OH)_4]}^- \quad 39.4^2$ $\text{pGa} \quad 30.0$
Speciation plots	
	

Table S3. Conditional formation constants for the Ga(III) and Fe(III) complexes of THP^H. Detailed species and chemical equations for which the constants were determined are defined below. Speciation plots are also reported for [L]_{total} = 10 μM and [M]_{total} = 1 μM (gallium complex) and [L]_{total} = 20 μM, [M]_{total} = 20 μM and [EDTA]_{total} = 50 mM (iron complex).

THP^H			
			
Chemical equilibrium equations			
$M^{3+} + L^{6-} + 3 H^+ \rightleftharpoons [MLH_3]$	$\text{Log } \beta_{[MLH_3]}^*$		
$M^{3+} + L^{6-} \rightleftharpoons [ML]^{3-}$	$\text{Log } \beta_{[ML]^{3-}}$		
$M^{3+} + 4 OH^- \rightleftharpoons [M(OH)_4]^-$	$\text{Log } \beta_{[M(OH)_4]^-}$		
$Fe^{3+} + EDTA^{4-} + 2 OH^- \rightleftharpoons [FeEDTA(OH)_2]^{3-}$	$\text{Log } \beta_{[FeEDTA(OH)_2]^{3-}}$		
Conditional formation constants			
$\text{Log } \beta_{[FeLH_3]}$	72.9*	$\text{Log } \beta_{[GaLH_3]}$	76.2*
$\text{Log } \beta_{[FeL]^{3-}}$	40.9	$\text{Log } \beta_{[GaL]^{3-}}$	42.5
$\text{Log } \beta_{[Fe(OH)_4]^-}$	34.4 ²	$\text{Log } \beta_{[Ga(OH)_4]^-}$	39.4 ²
$\text{Log } \beta_{[FeEDTA(OH)_2]^{3-}}$	42.0 ²	pGa	31.8
pFe	28.6		
Speciation plots			
			

* Because only intrinsic metal complex protonation⁴ can be discriminated using this method, the cumulative 3 protons metal complex formation constant was fitted with the data with no further stepwise constant fitting.

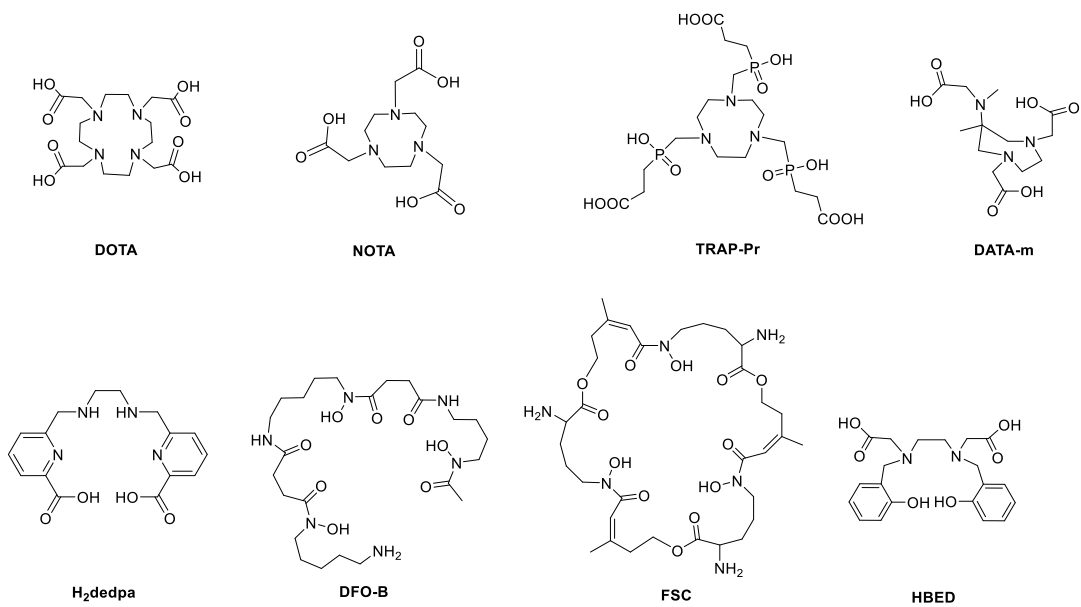


Figure S1. Chemical structures of selected Ga^{3+} chelators evaluated for use with ^{68}Ga .

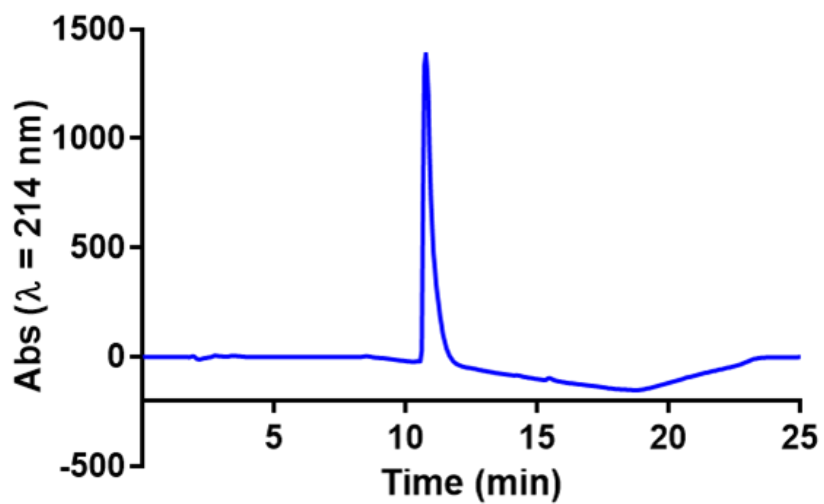


Figure S2. UV Chromatogram ($\lambda = 214$ nm) of THP^H using HPLC method 5.

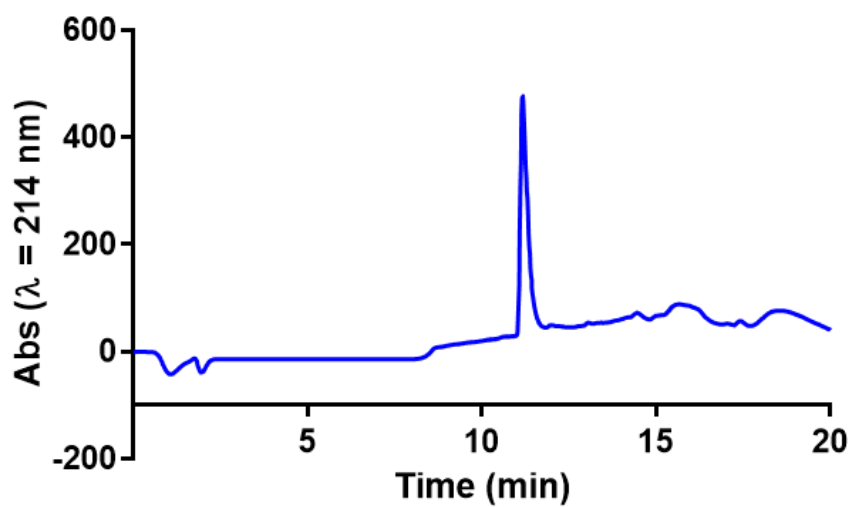


Figure S3. UV Chromatogram ($\lambda = 214$ nm) of THPO using HPLC method 6.

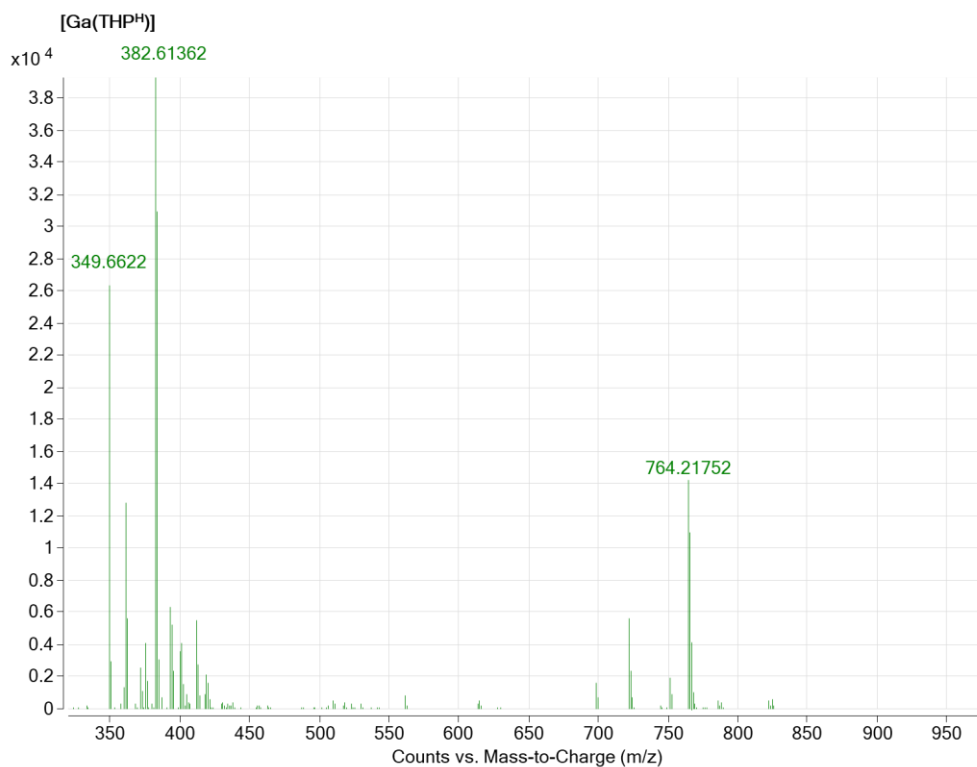


Figure S4. ESI mass spectrum for the $[Ga(THP^H)]$ complex. The peak at 764.22 m/z represents $[Ga(THP^H)+H]^+$ and shows the typical isotopic pattern of a natural gallium complex. Peak at 382.61 and 349.67 are assigned to the doubly-charged species $[Ga(THP^H)+2H]^{2+}$ and $[THP^H+2H]^{2+}$, respectively. The minor peak at 698.32 represents $[THP^H+H]^+$, peaks at 720.29 and 751.23 m/z are assigned to the sodium and iron complex of THP^H , respectively. No peaks assignable to stoichiometry other than 1:1 were visible.

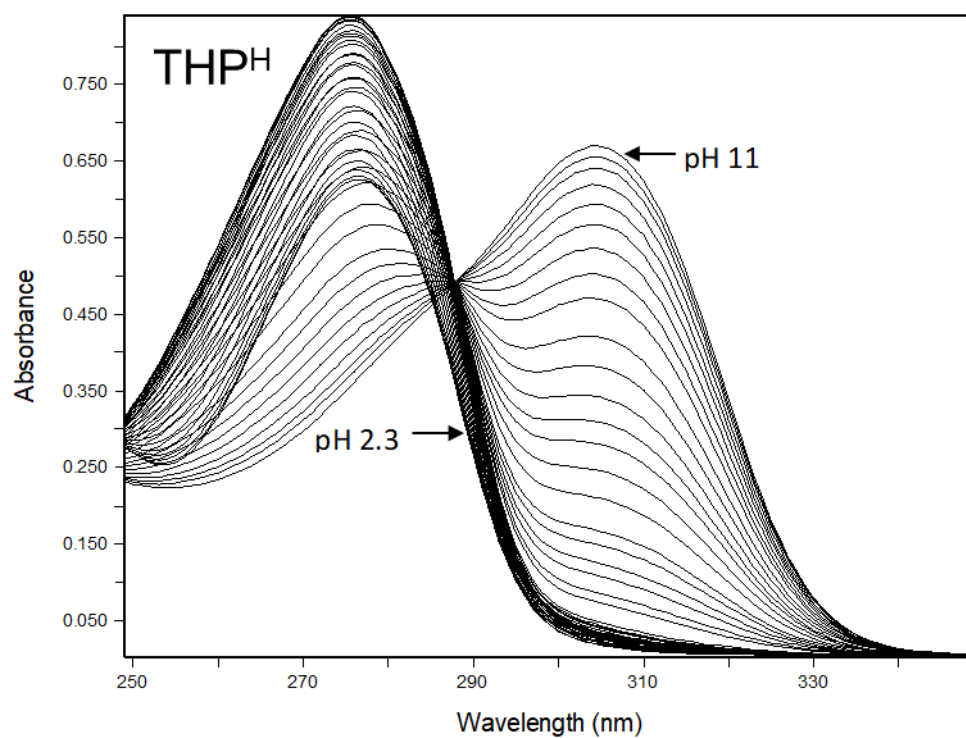
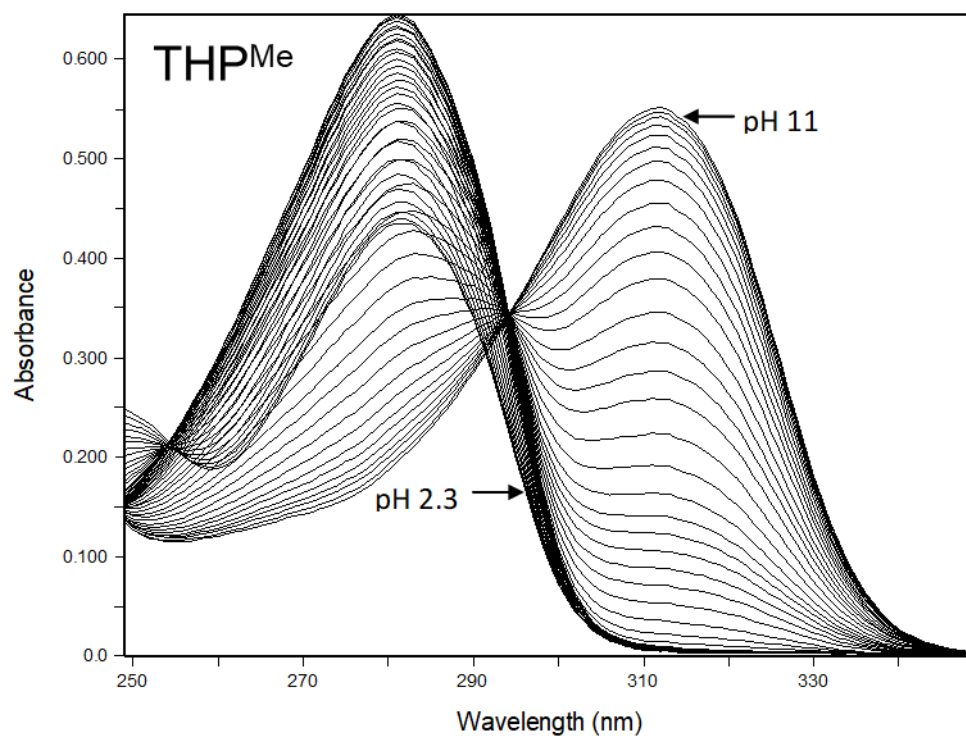


Figure S5. Absorbance spectra of THP^{Me} and THP^H ($\lambda_{range} = 250-400$ nm) at different pH values (intervals of 0.1 pH unit).

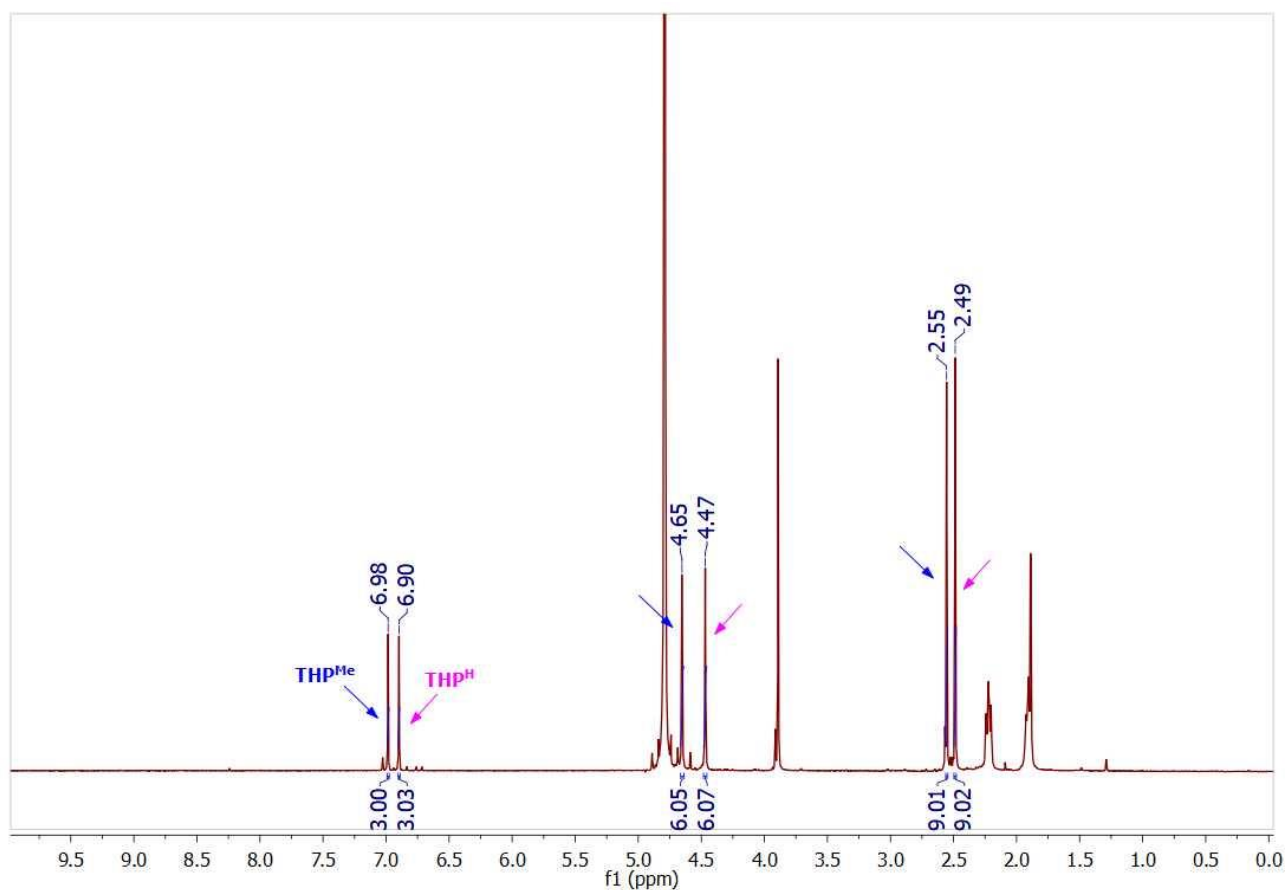


Figure S6. ^1H NMR of a solution 2 mM in THP^{Me} and 2 mM in THP^H in D₂O. Peaks are referenced to residual solvent signal. Pink and blue arrows indicate signals from THP^H and THP^{Me}, respectively. Peak integration is reported (from left to right) for the pyridinone C⁵-H hydrogen, the C²-CH₂-NH₂ group and the C⁶-CH₃, confirming equal concentration of the two ligands.

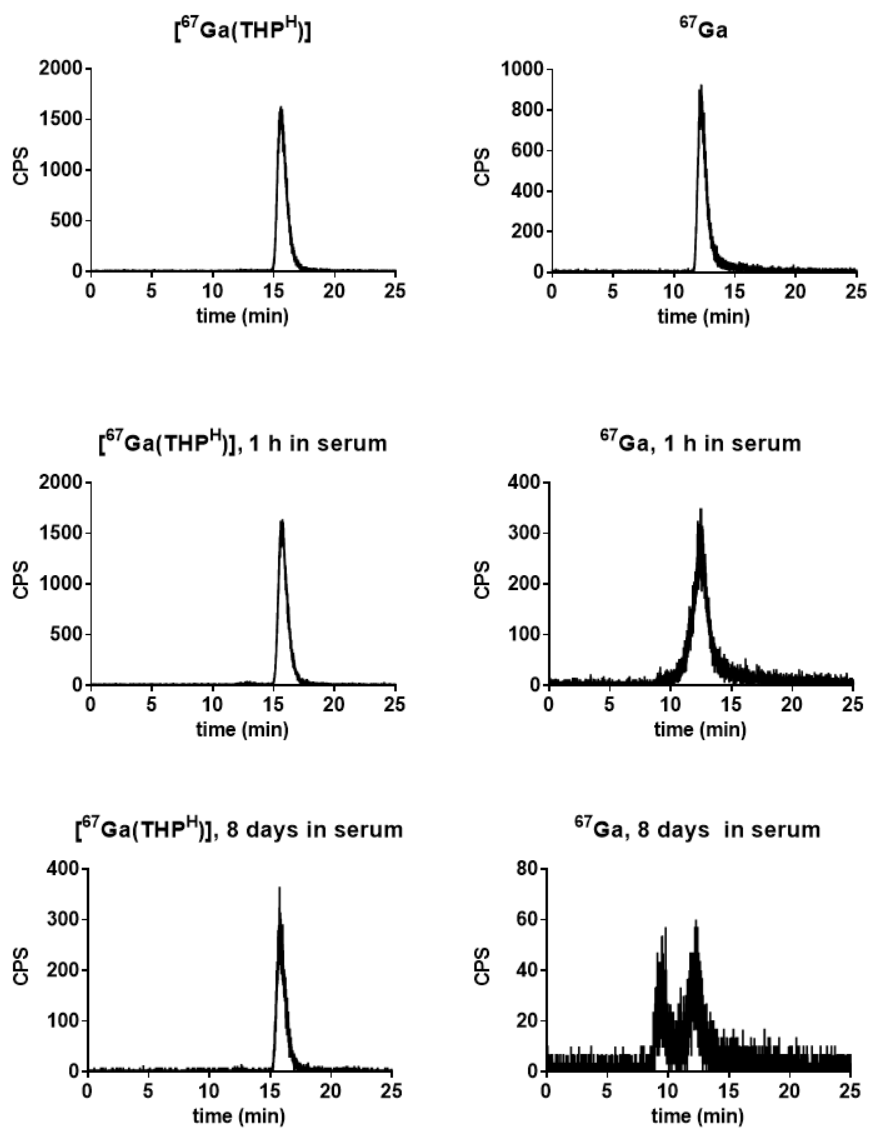


Figure S7. Size-exclusion radiochromatograms of $[^{67}\text{Ga}(\text{THP}^{\text{H}})]$ and ^{67}Ga without human serum and after incubation with human serum at 37 °C at 1 hour and up to 8 days.

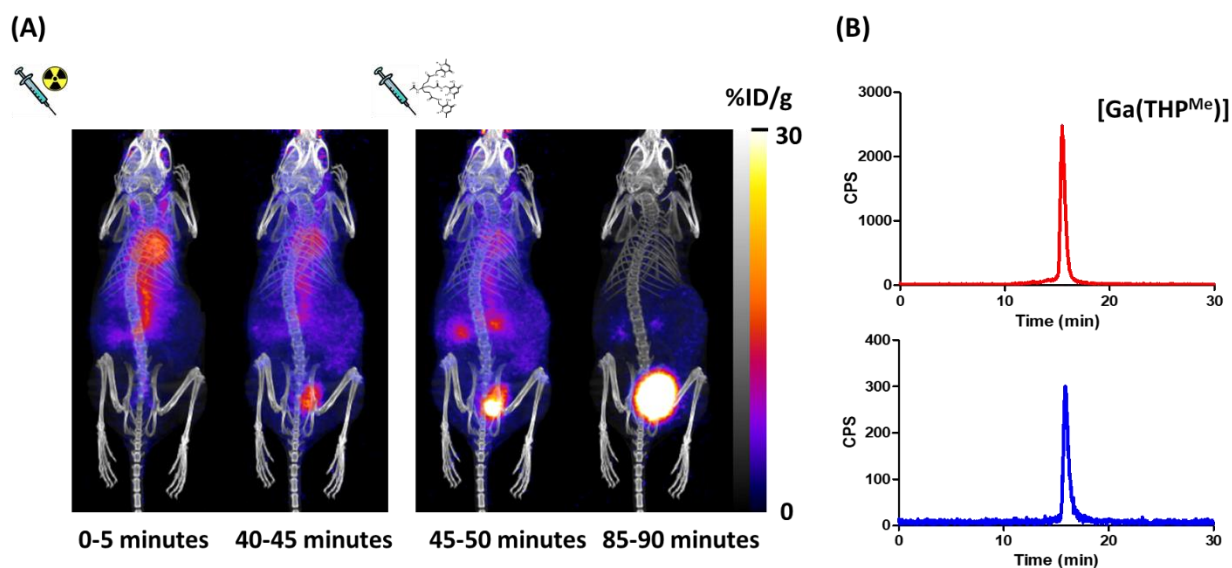


Figure S8. A) Dynamic PET/CT MIP, at different time points, of a mouse injected with acetate buffered ^{68}Ga at time 0 followed by THP^{Me} at 45 minutes. A sudden change in the biodistribution of ^{68}Ga is visible soon after injection of the chelator, with the blood pool activity quickly clearing through the kidneys into the bladder. B) Comparison of the radiochromatograms of $[^{68}\text{Ga}(\text{THP}^{\text{Me}})]$ (top panel) and of the mouse urine at 90 minutes after ^{68}Ga injection (bottom panel), demonstrating in vivo formation of $[^{68}\text{Ga}(\text{THP}^{\text{Me}})]$ following THP^{Me} administration (reversed-phase HPLC, method 3).

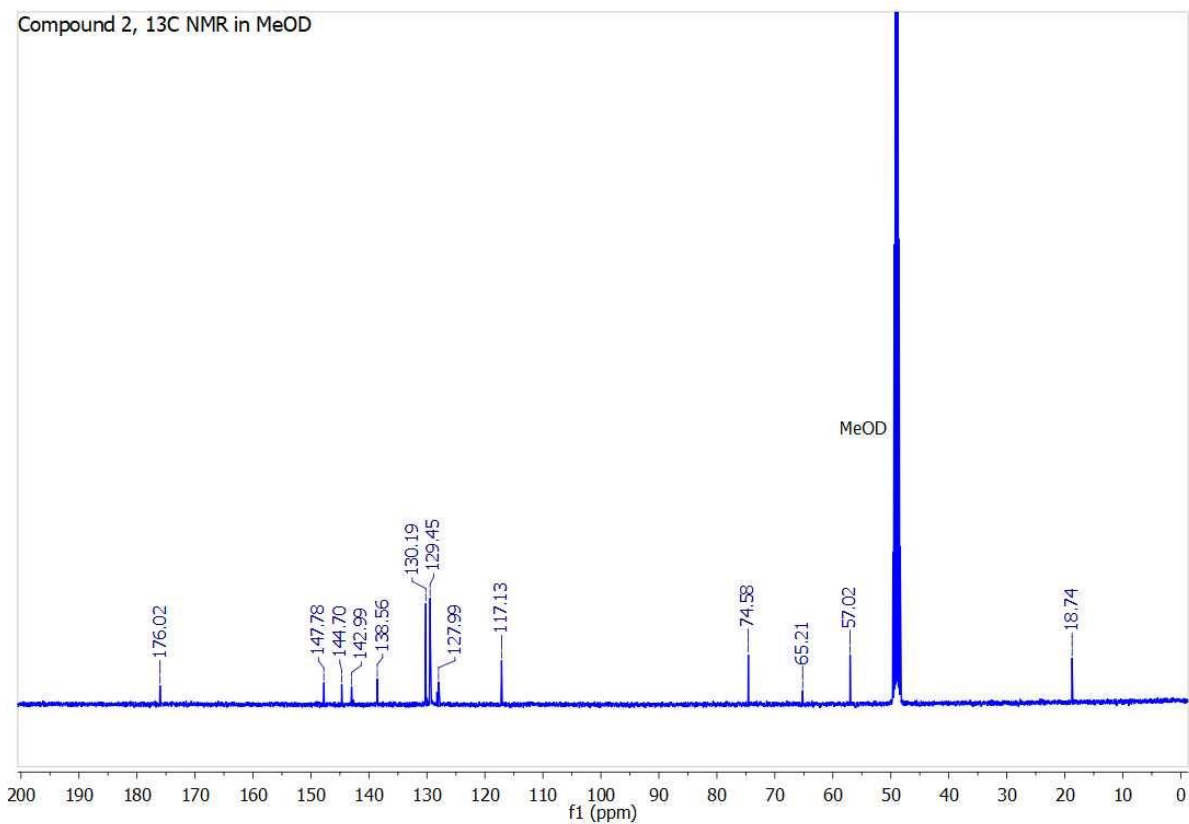
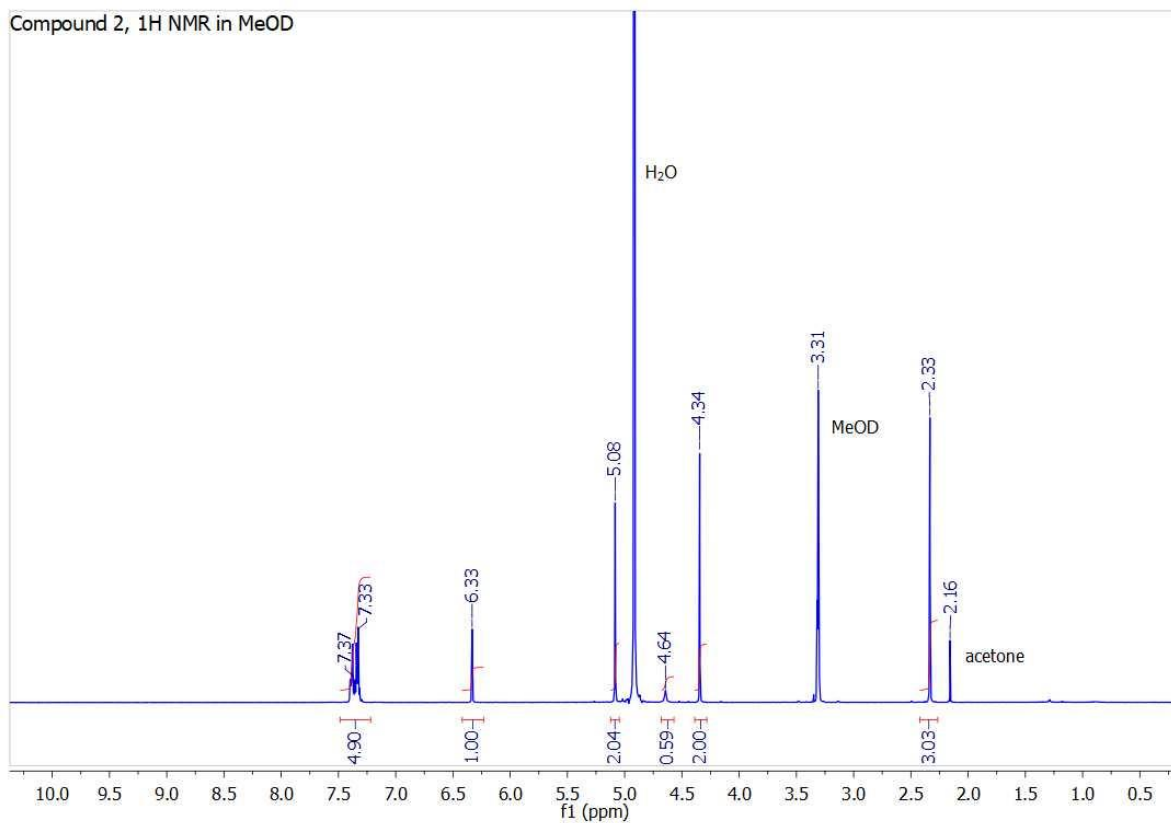


Figure S9. ^1H NMR (top panel) and ^{13}C NMR (bottom panel) of **2** in methanol- d_4 .

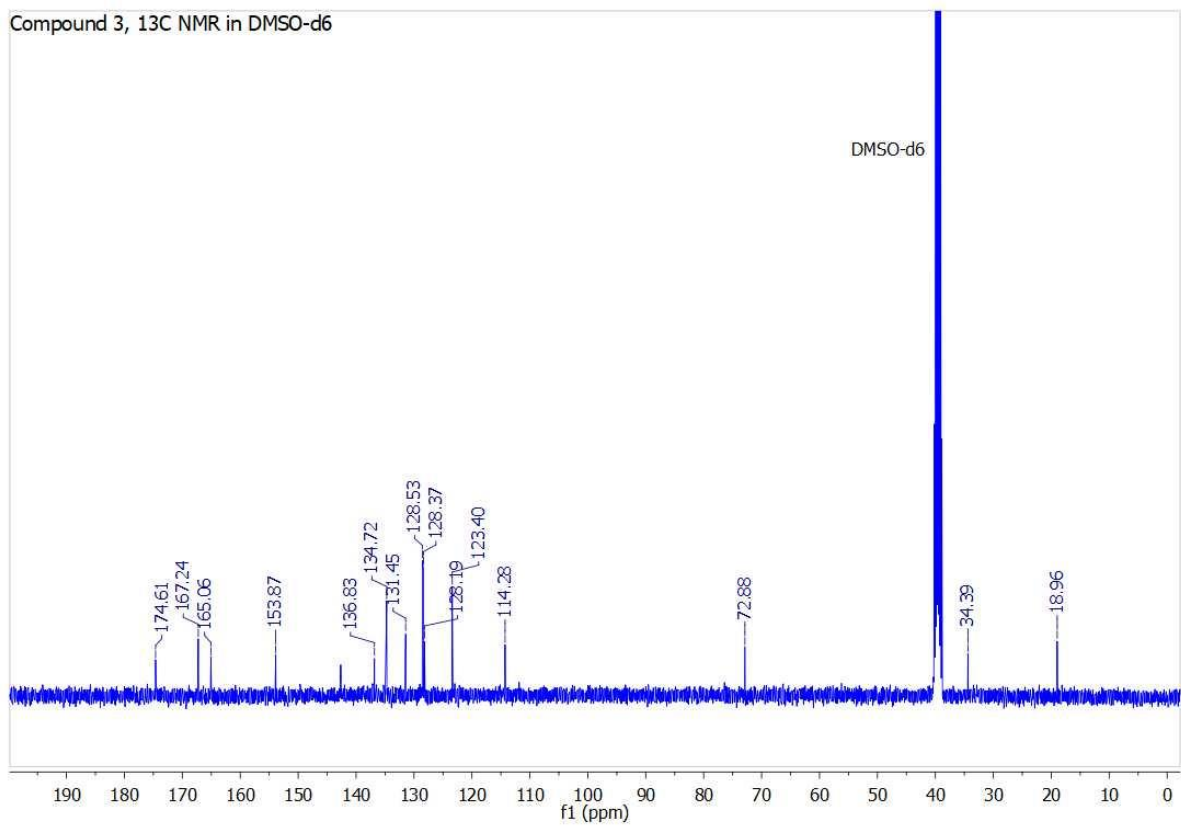
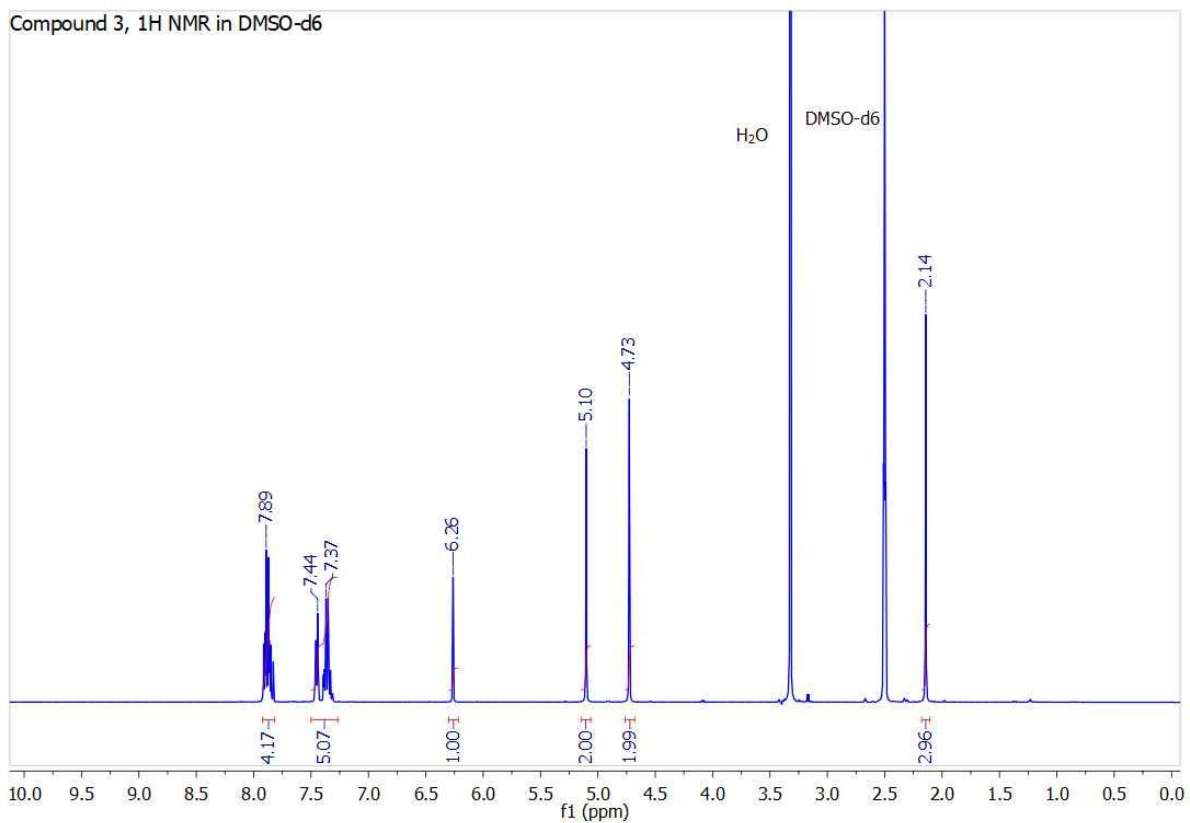


Figure S10. ^1H NMR (top panel) and ^{13}C NMR (bottom panel) of **3** in DMSO- d_6 .

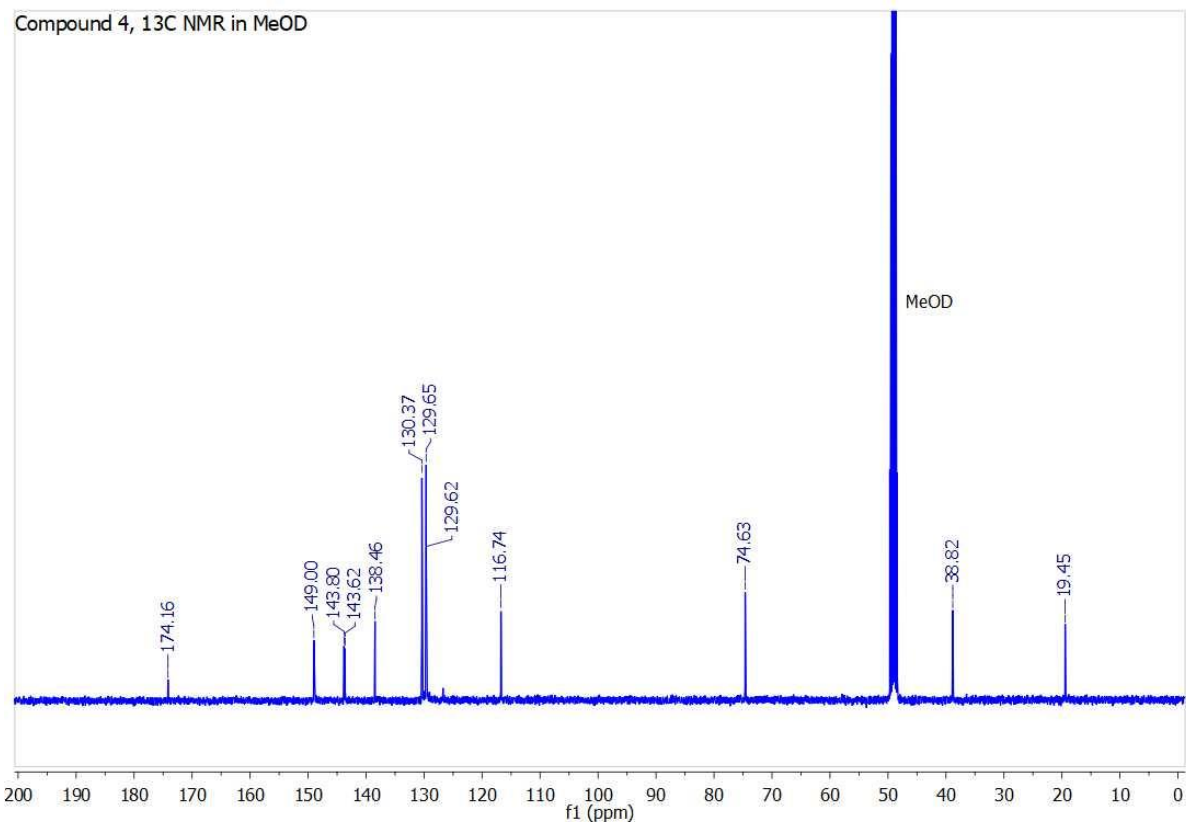
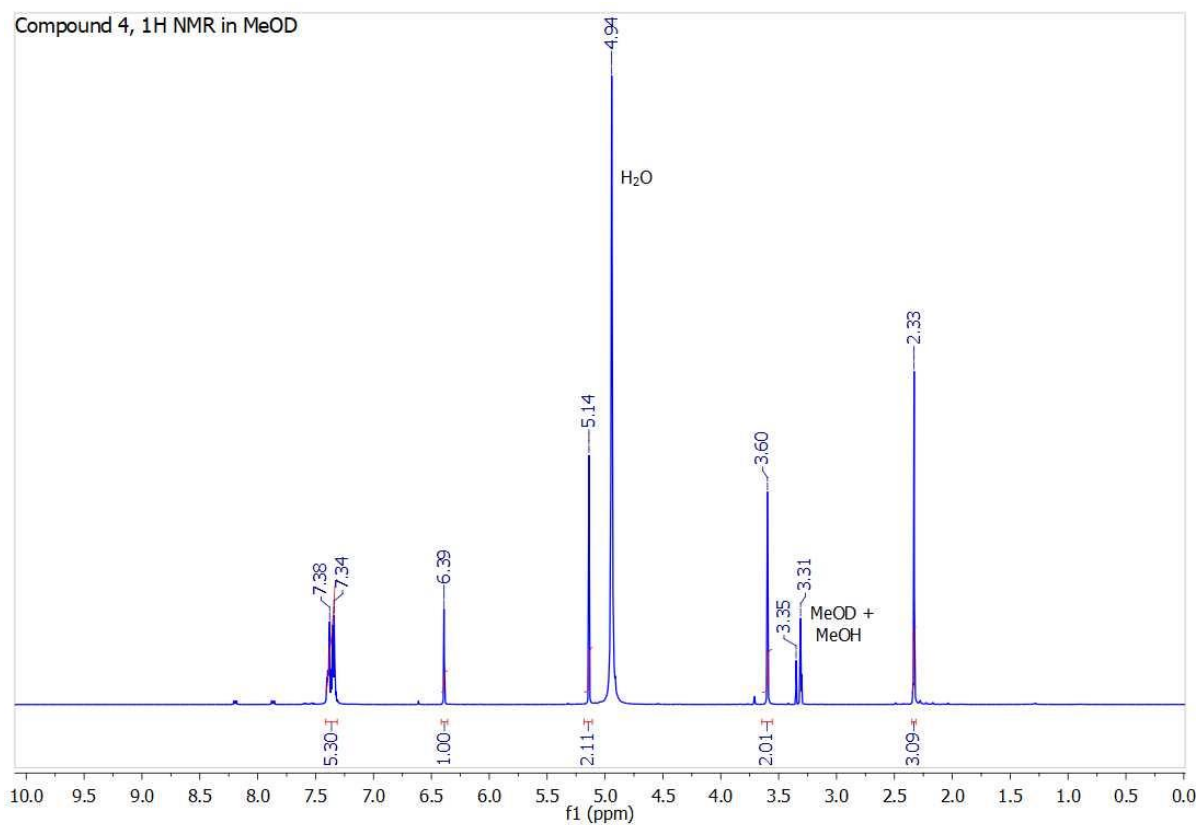


Figure S11. ^1H NMR (top panel) and ^{13}C NMR (bottom panel) of **4** in methanol- d_4 .

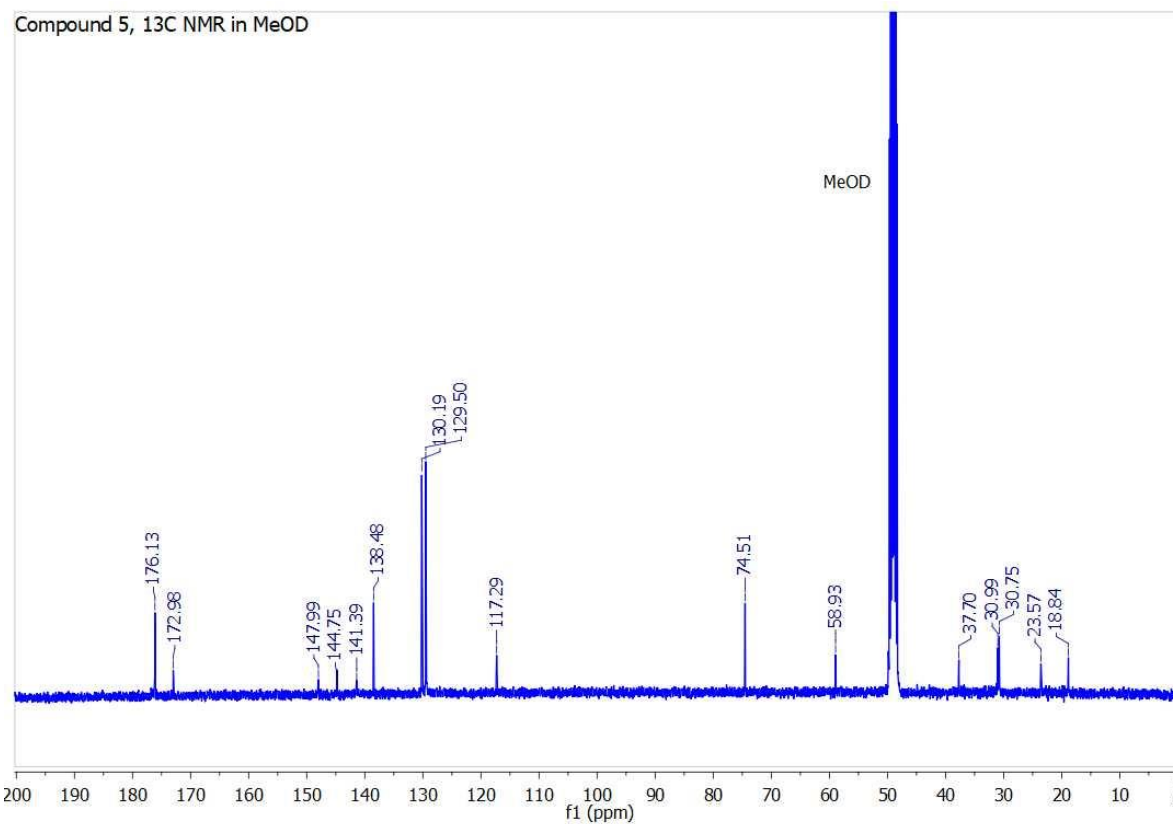
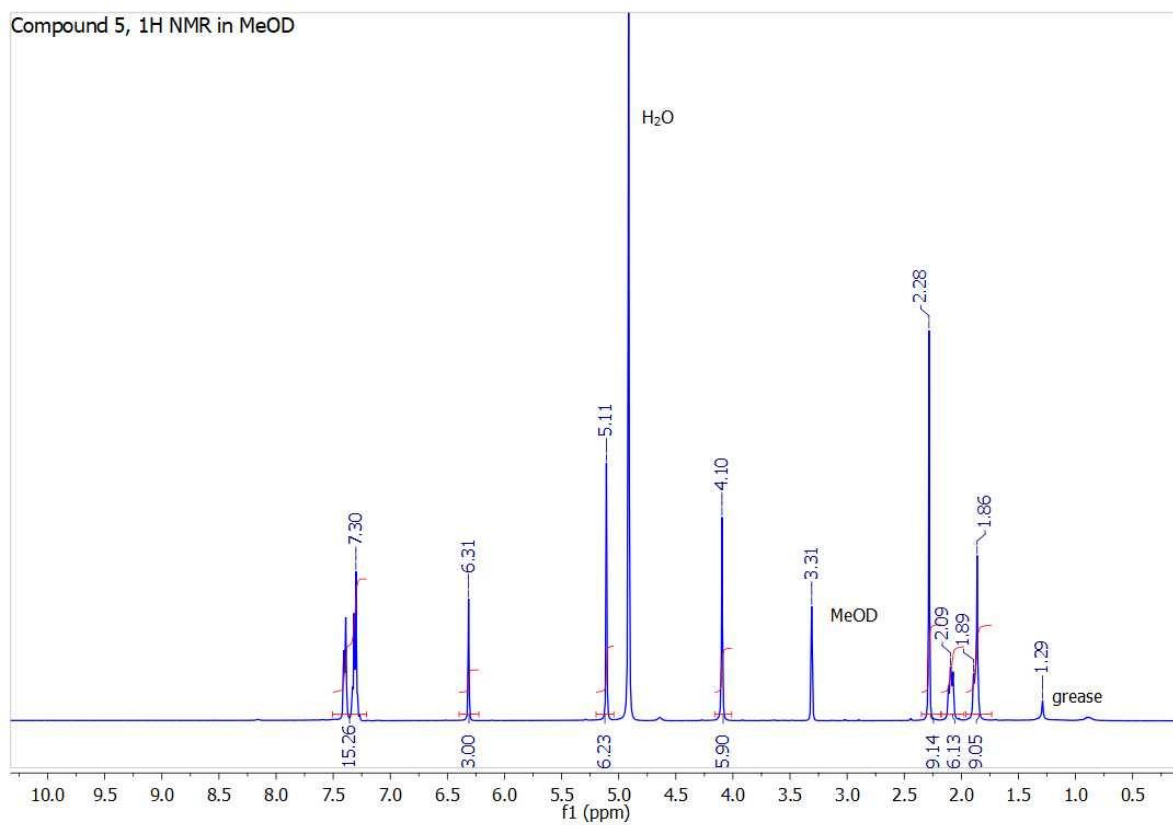


Figure S12. ^1H NMR (top panel) and ^{13}C NMR (bottom panel) of **5** in methanol- d_4 .

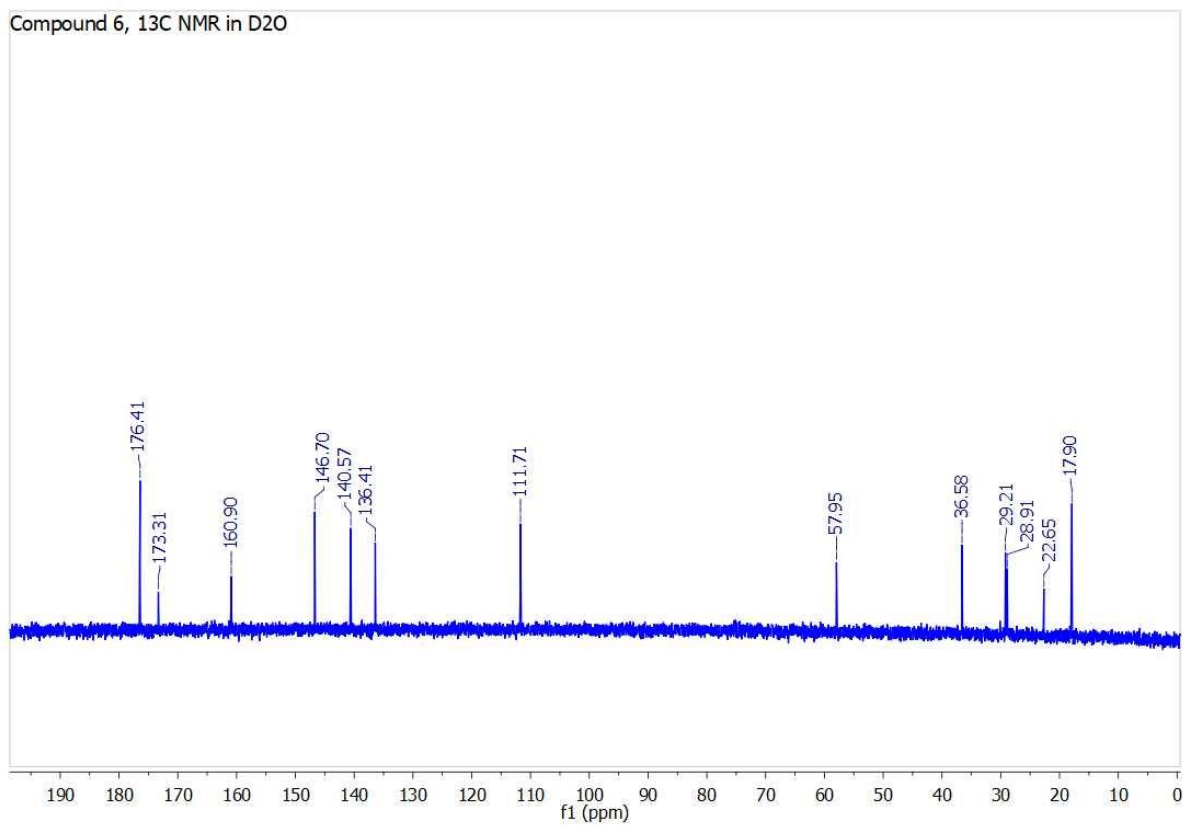
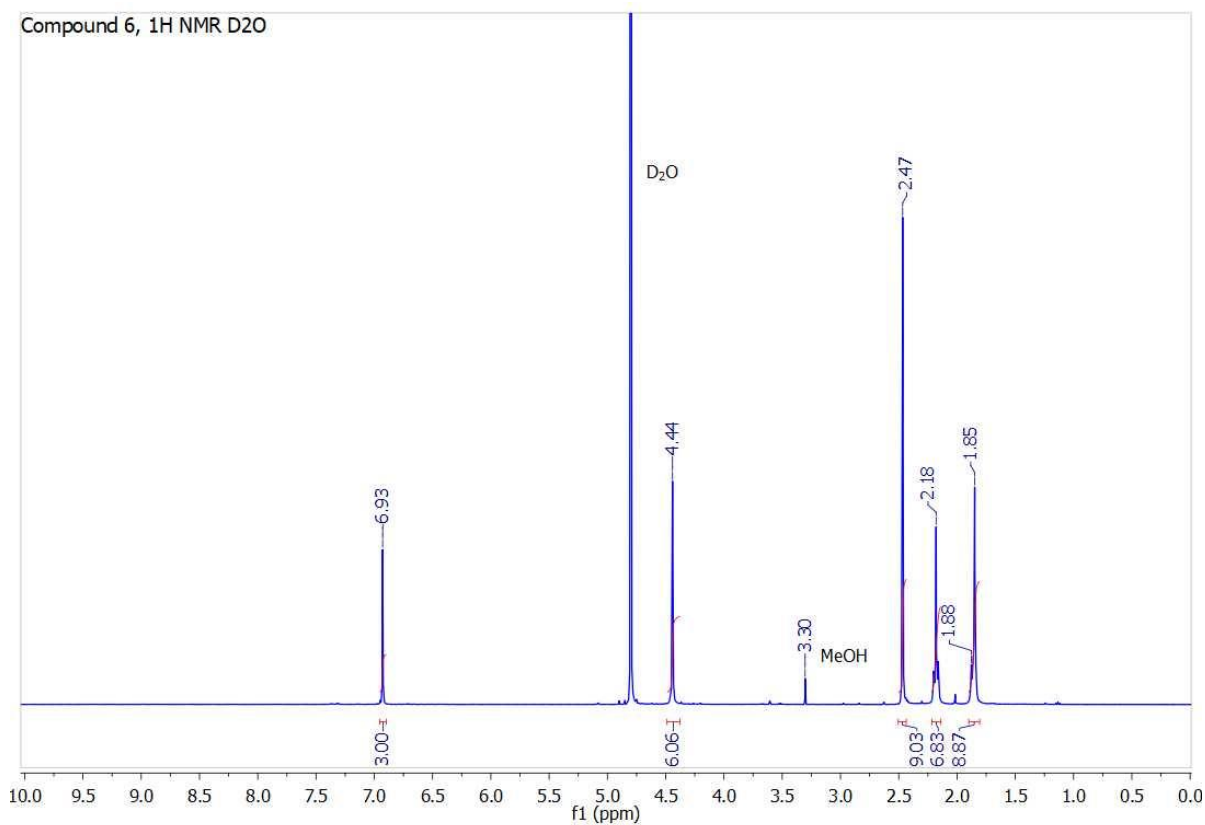


Figure S13. ^1H NMR (top panel) and ^{13}C NMR (bottom panel) of **6** in D_2O .

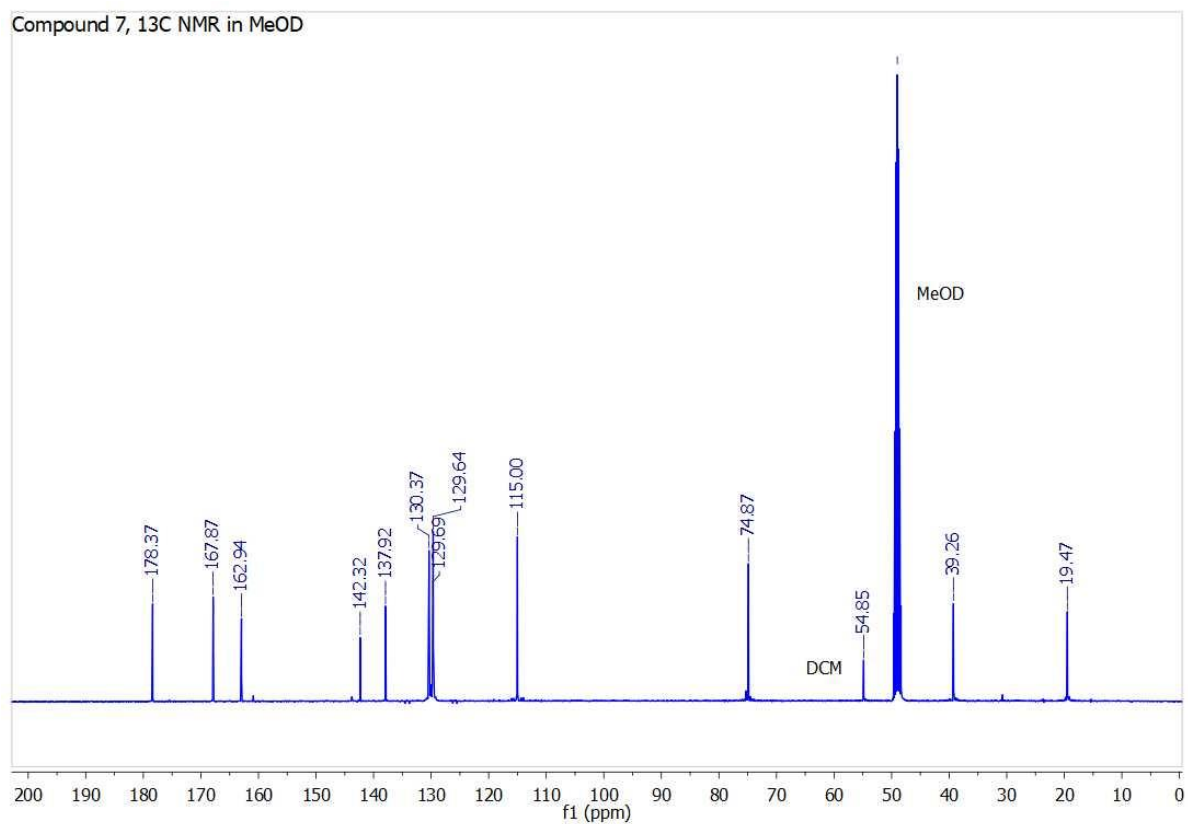
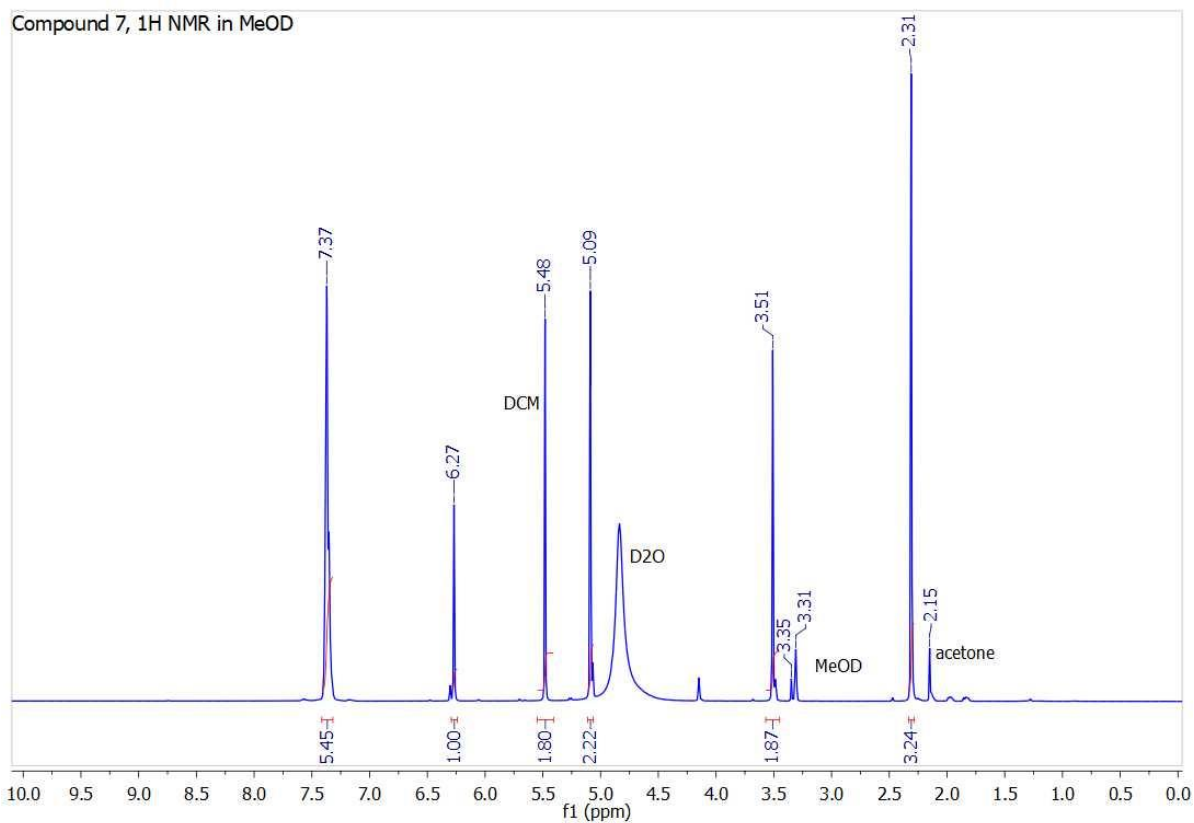


Figure S14. ^1H NMR (top panel) and ^{13}C NMR (bottom panel) of **7** in methanol- d_4 .

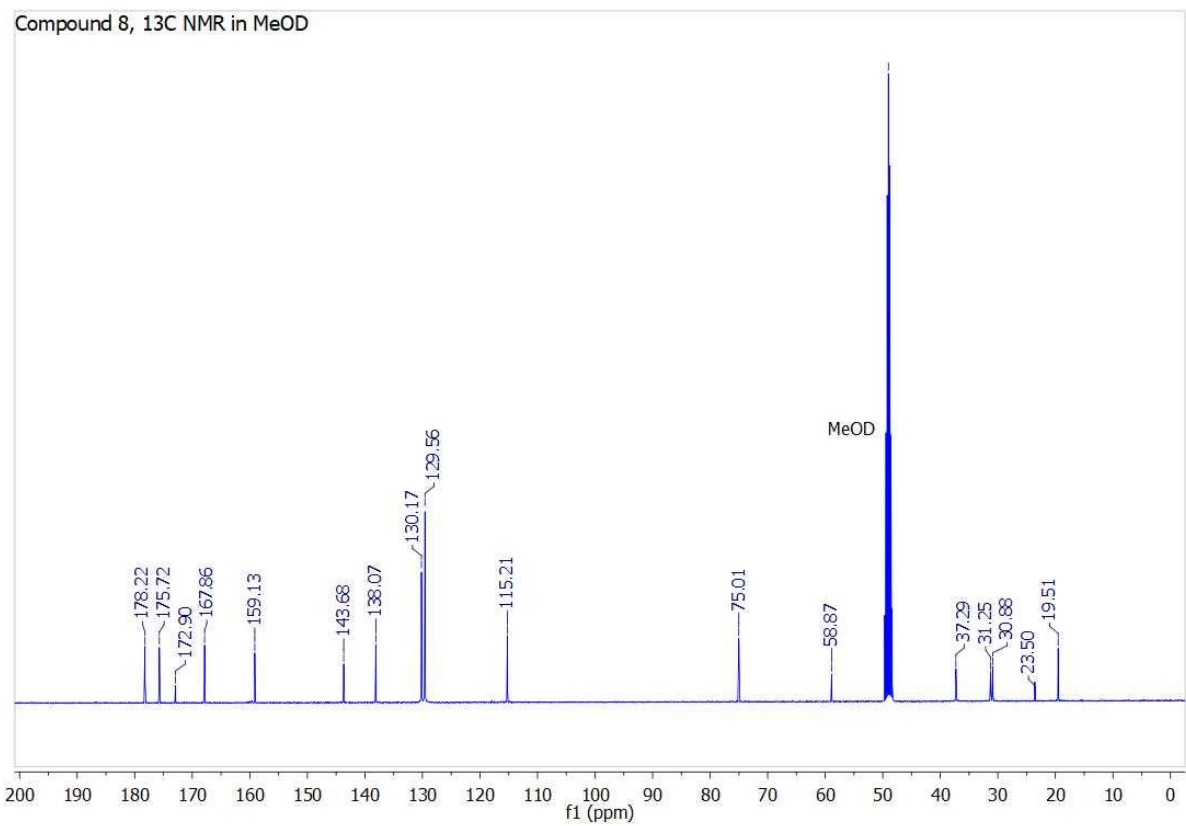
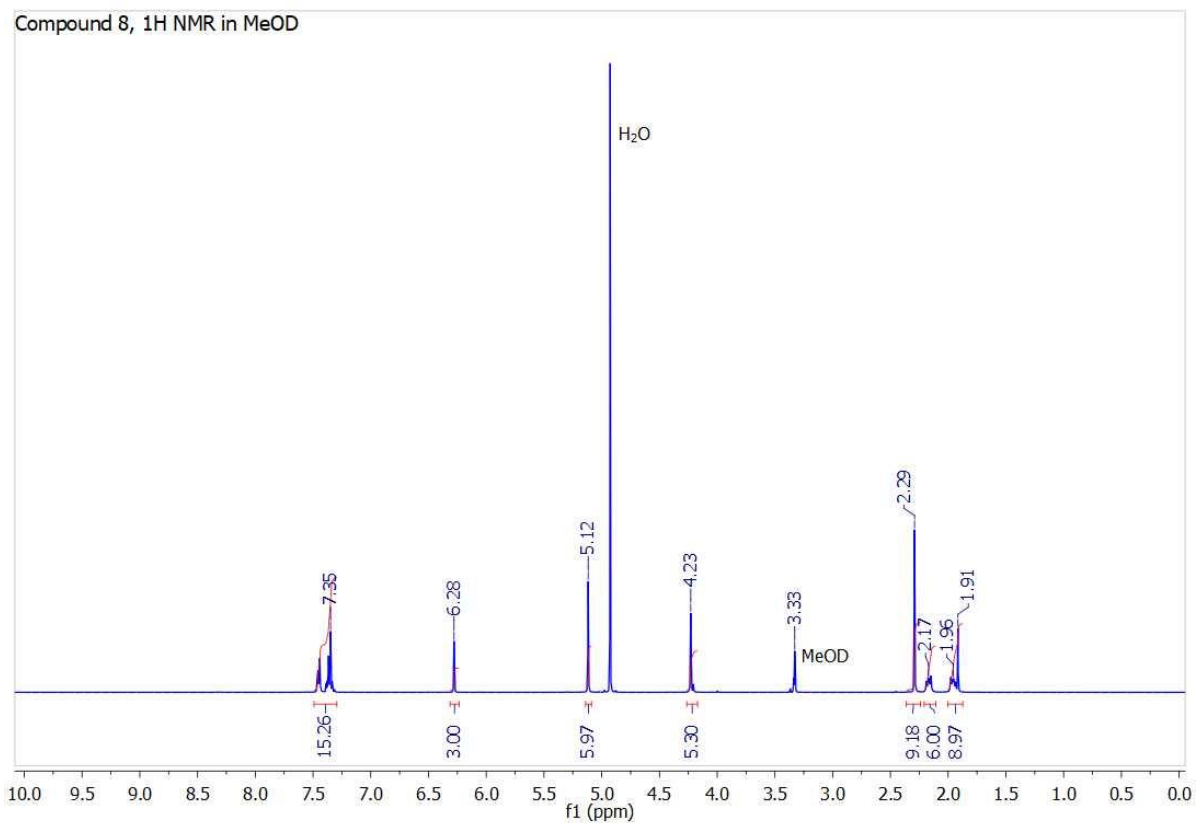


Figure S15. ^1H NMR (top panel) and ^{13}C NMR (bottom panel) of **8** in methanol- d_4 .

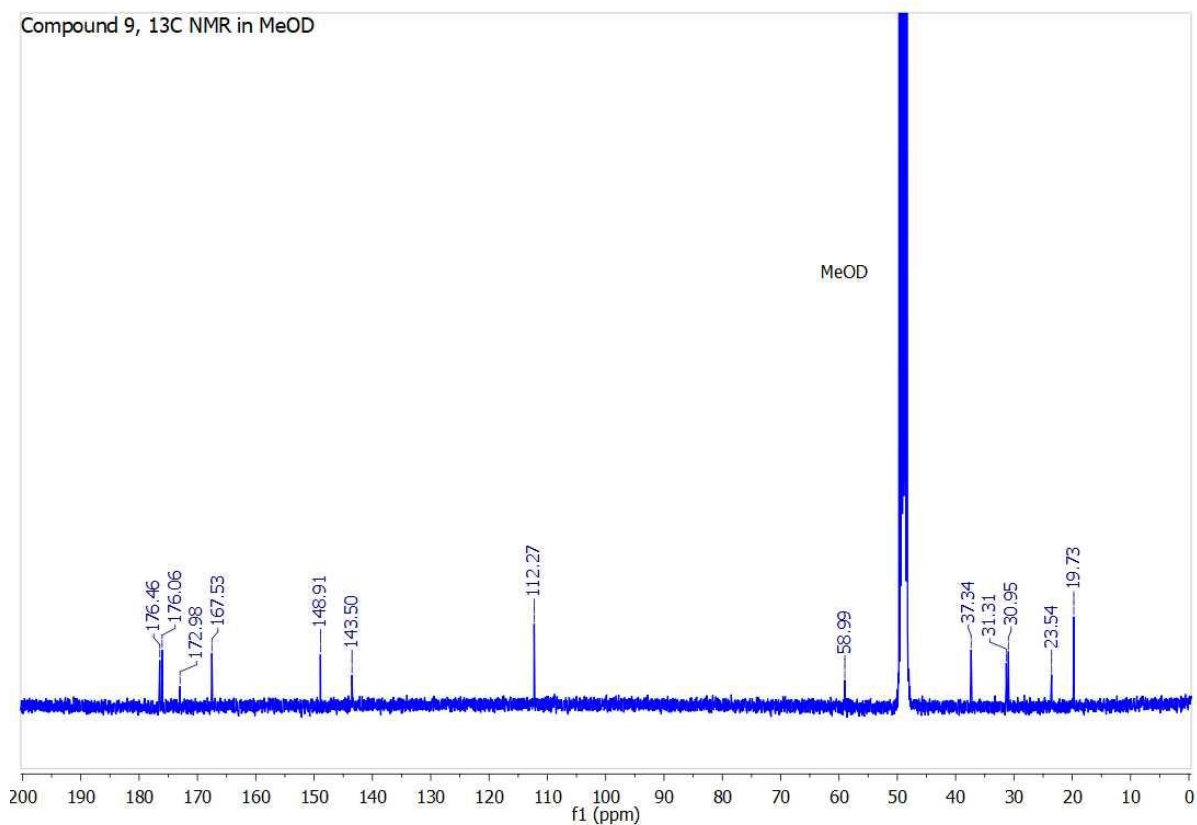
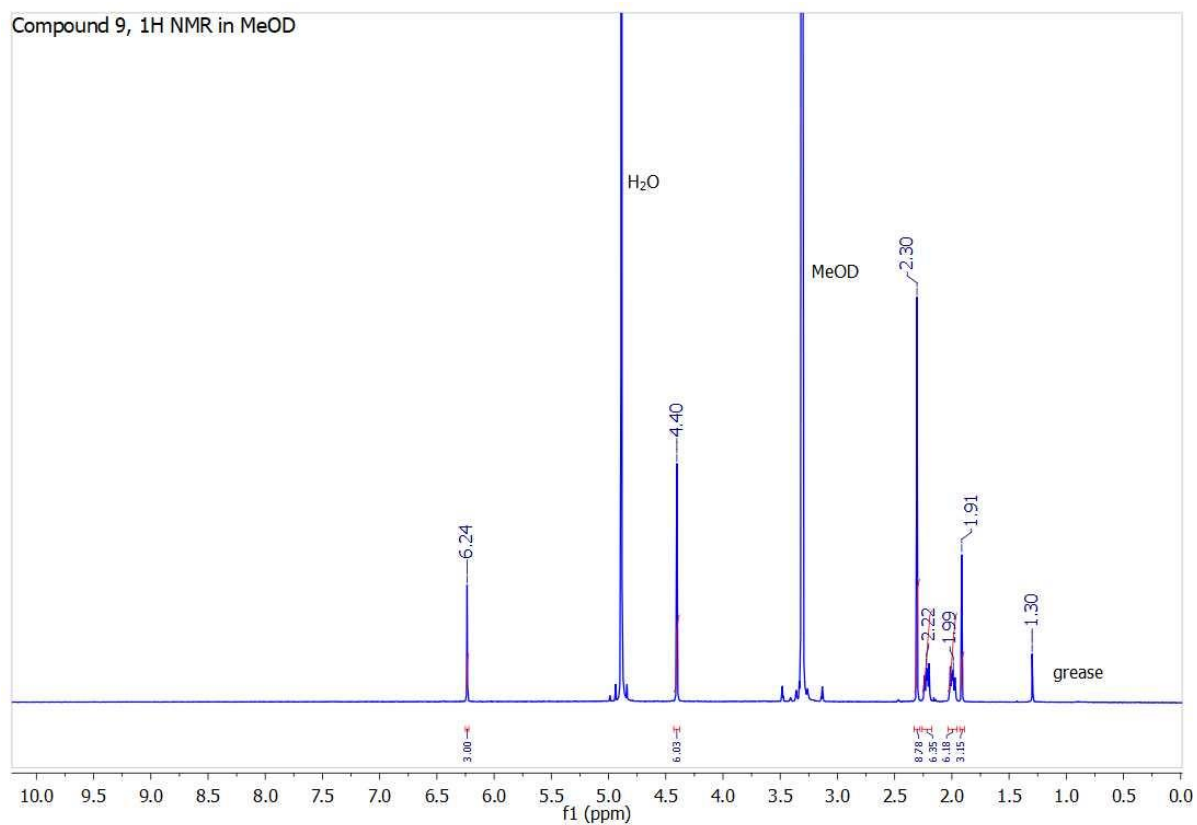


Figure S16. ^1H NMR (top panel) and ^{13}C NMR (bottom panel) of **9** in methanol- d_4 .

References

1. S. Nawaz, PhD thesis, King's College London, 2013.
2. E. A. Martell and R. M. Smith, *Critical Stability Constants*, Plenum Press, New York, 1977-1989.
3. R. Cusnir, C. Imberti, P. J. Blower, M. T. Ma and R. C. Hider, *Int J Mol Sci*, 2017, 18, 116.
4. P. D. Taylor, *Talanta*, 1995, **42**, 845-850.